JOURNAL OF GUIDANCE, CONTROL, AND DYNAMICS
Vol. 32, No. 1, January–February 2009

Sensor Fusion Applied to Autonomous Aerial Refueling

Walton R. Williamson,* Gregory J. Glenn,† Vu T. Dang,‡ and Jason L. Speyer§
SySense, Inc., Burbank, California 91502
and
Stephen M. Stecko¶ and John M. Takacs**
The Boeing Company, Long Beach, California 90807

DOI: 10.2514/1.34589

A methodology for performing sensor fusion using differential Global Positioning System receivers, inertial measurements, wireless communication, and electro-optical measurements is presented. An estimation structure based on an extended Kalman filter is developed to estimate the precise relative position, velocity, and attitude of two aircraft flying in close proximity. The project is focused on the development of this methodology for automatic aerial refueling in which a boom control system uses the output of the sensor fusion to guide the boom into the receiver receptacle. Results from a real-time, hardware-in-the-loop demonstration are presented which show estimator performance and feedback control capability on a scaled model.

Nomenclature

a^B	=	inertial acceleration vector of the vehicle in the body frame
b_c^i	=	Global Positioning System common mode errors for satellite i
$C_{\bar{B}}^A$	=	a priori estimate of the cosine rotation matrix to rotate a vector from the B frame to the A frame
G	=	Earth gravity gradient matrix representing gravity variations in the Earth-centered, Earth-fixed coordinate frame
g^E	=	Earth gravity vector represented in the Earth-centered, Earth-fixed coordinate frame
L_{I2G}	=	lever arm from the inertial measurement unit to the Global Positioning System antenna represented in the body frame
N_1^i	=	integer number of Global Positioning System carrier wavelengths between satellite i and receiver 1
P^E	=	position vector in the Earth-centered, Earth Fixed coordinate frame
$\tilde{P}_{\text{GPS}}^E$	=	measurement of the Earth-centered, Earth-fixed position of the Global Positioning System antenna
$\bar{P}_{\text{IMU}}^E$	=	a priori estimate of the Earth-centered, Earth-fixed position of the inertial measurement unit
Q_B^A	=	quaternion representation of a rotation from the B reference frame to the A frame
$Q_B^A \otimes Q_C^B$	=	quaternion rotation from C frame to A frame
V^E	=	velocity vector in the Earth-centered, Earth-fixed coordinate frame
$v_{\phi 1}^i$	=	Global Positioning System receiver 1 carrier-phase measurement noise for satellite i
υ_α	=	elevation angle measurement noise
υ_β	=	azimuth angle measurement noise
w_a	=	accelerometer white noise
w_g	=	gyro white noise
$\dot{x}$	=	time derivative of the vector x
$\bar{x}$	=	a priori estimate of the parameter x
$\hat{x}$	=	a posteriori estimate of the parameter x
$\tilde{x}$	=	measurement of the parameter x
x_1	=	parameter relating to vehicle 1
x_2	=	parameter relating to vehicle 2
$\|x\|$	=	L2-norm of the vector x
$\tilde{\alpha}_{iC}$	=	elevation angle from vehicle 1 electro-optic sensor frame to reference point i on vehicle 2
$\tilde{\beta}_{iC}$	=	azimuth angle from vehicle 1 electro-optic sensor frame to reference point i on vehicle 2
δx	=	perturbation about the parameter x (truth minus a priori estimate)
$\delta\Delta x$	=	perturbation error in the relative navigation state (vehicle 1 minus vehicle 2)
λ	=	Global Positioning System carrier-phase wavelength
ρ_1^i	=	true range from satellite i to vehicle 1
ϕ_1^i	=	Global Positioning System carrier-phase measurement for satellite i measured at vehicle 1
ω_{AB}^C	=	angular velocity of B fame relative to the A frame represented in the C frame
$[\omega\times]$	=	cross-product matrix representation of the vector ω
$\nabla\Delta\phi$	=	double-differenced carrier-phase measurements
$\nabla\Delta N$	=	double-differenced carrier-phase integer ambiguity

Received 14 September 2007; revision received 2 June 2008; accepted for publication 8 July 2008.

*Research Engineer, 300 East Magnolia, Suite 300. AIAA Member.
†Engineer, 300 East Magnolia, Suite 300.
‡Software Engineer, 300 East Magnolia, Suite 300.
§Chief Science Officer, 300 East Magnolia, Suite 300. AIAA Fellow.
¶Manager of Advanced Aerial Refueling Systems, Boeing Integrated Defensive Systems, 2401 East Wardlow Road.
**Senior Principal Engineer Electro-Optics, Boeing Integrated Defense Systems, 2600 Westminster Boulevard, SL-13, Seal Beach, California 90740.

I. Introduction

THIS paper focuses on the development and implementation of a methodology for relative navigation between two vehicles and specifically addresses the problem of automatic in-flight refueling between a tanker and receiver. We develop a high-accuracy and redundant navigation system to estimate the position, velocity, and attitude of each vehicle relative to the other in real time. The instruments selected for this demonstration include inertial navigation, electro-optic (EO) image sensors, a wireless communication system, and differential carrier-phase (DCP) Global Positioning System (GPS) receivers. A sensor fusion process is presented using an extended Kalman filter (EKF) which uses either the GPS or the EO sensors to correct the inertial navigation state of both vehicles. The navigation system was tested in a hardware-in-the-loop (HITL) environment simulating boom-style aerial refueling. An automatic feedback control demonstrated that the

real-time navigation state could be used to guide the boom model into the receiver receptacle in the HITL environment.

It is shown that the system is redundant because either the GPS or EO sensor may be used to provide corrections to the relative inertial navigation state. If differential GPS measurements are lost due to jamming or blockage, then the tanker relies on the EO system to provide corrections to the relative navigation state. Likewise, if the EO system is unavailable, the differential GPS measurements may be used to correct the states. If both the EO sensor and GPS are unavailable, then the inertial system of each aircraft can be used to coast through the outage to complete refueling or move to a minimum safe distance. The present demonstration assumes the receiver transmits information to the tanker and the tanker performs the sensor fusion process to provide a high-accuracy estimate of the receiver receptacle location to the tanker boom control system, although the information flow could be reversed to enable the receiver to perform position tracking relative to the tanker.

II. Sensor Fusion Overview

The key technology components demonstrated are depicted in block diagram form in Fig. 1. In this figure, the shaded blocks are located on the tanker and the clear blocks are located on the receiver aircraft. The receiver aircraft uses an onboard GPS and inertial measurement unit (IMU) to estimate the vehicle position, velocity, attitude, angular rate, and acceleration. These measurements and states are transmitted to the tanker aircraft across a wireless data link. The tanker also uses an onboard GPS and IMU to estimate the tanker position, velocity, attitude, acceleration, and angular rate. The tanker navigation system corrects the inertial data with differential carrier-phase GPS data through an EKF to form the precise relative state vector between the two vehicles. The tanker uses an electro-optic sensor to provide bearings measurements to a set of known reference points on the receiver. Each reference point location is known relative to the receiver aircraft IMU. A silhouette-matching approach may also be used to estimate the range, bearings, and attitude of the receiver. The sensor fusion process then uses the EO measurements to correct the inertial estimates. The background of the development of each of the modules required to complete this process is briefly described in this section.

A. Global Positioning System and Inertial Sensor Fusion

The work presented herein builds on previous methods of autonomous formation flight, landing, and aerial refueling. Methods for blending a GPS receiver and an inertial system have been demonstrated previously [1]. A method for using differential carrier-phase GPS measurements to correct two inertial navigation systems (INS) [1] was demonstrated using two F-18 aircraft at NASA Dryden Flight Research Center. That work showed the capability to resolve the differential carrier-phase GPS integer ambiguity problem [2] in real time and provided a methodology for correcting the inertial state of each vehicle. The output of the integer ambiguity algorithm was fused with the INS data from each aircraft through a suboptimal EKF [1,3] to provide relative position, velocity, and attitude estimates of each vehicle. EKF structures generated using the GPS measurements and linearized error dynamics of the INS are only completely observable in the presence of dynamics. Without vehicle motion, estimates of the errors in yaw and yaw bias are unobservable as discussed in Hong et al. [4].

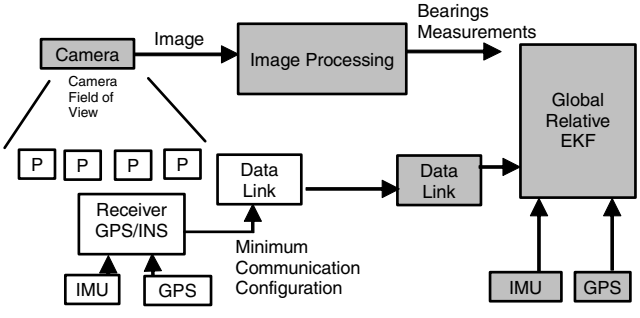

Fig. 1 GPS/INS/EO sensor fusion block diagram.

In the F-18 flight tests, relative position estimates were shown to be accurate to centimeter level [3,5]. Two methods for fusing the GPS and inertial data were explored: a filter which estimated the state errors in both vehicles, and a reduced-order filter that only estimated the relative state estimates. The reduced-order method was implemented as a compromise due to computational limits available at the time. For this filter, the leader vehicle provided a corrected GPS/INS solution to the follower aircraft, and the follower aircraft EKF only estimated a state space consisting of the relative states between each vehicle linearized around the leader vehicle estimate. No feedback was provided to the leader sensor fusion process. In contrast, the work presented here supposes that the EKF sensor fusion process estimates both the leader vehicle state and the relative navigation state simultaneously. The filter structure is centralized on either the leader or follower aircraft, enabling all measurements to be used to form the best estimate of the state of both vehicles. The reduced-order method can still be shown to be a simplification of the EKF presented here. Because the reduced-order filter estimates only the relative state based on the leader state, whereas the centralized filter estimates all vehicle states in the estimation process, the centralized filter is referred to as the "global extended Kalman filter" (GEKF). The GEKF uses dynamics linearized about both vehicles' inertial state estimates and has improved estimation accuracy under high-dynamic conditions at the cost of increased computational power over the reduced-order estimator.

B. Global Positioning System Integer Ambiguity Resolution

The methodology used for differential GPS (DGPS) integer ambiguity resolution in the Autonomous Formation Flight experiment and in the present research is referred to as the Wald test [2], a hypothesis testing scheme which searches for estimating the correct integer combination from a set of possible integers. Other methods for GPS ambiguity resolution include the method attributed to Teunissen et al. [6] which has been applied to demonstrations of automated landing [7] for the Joint Precision Approach and Landing System. The methodology used an integer ambiguity resolution to provide centimeter level relative position between the F-18 and the carrier which was used to guide the aircraft to land on the carrier. The work presented in this paper uses the Wald test [2], which is preferred because it recursively calculates the probability that a particular hypothesis set is correct using the assumed statistical properties of the residuals. The advantage of this algorithm over other methods, such as integer boot strap, includes a more robust residual processing scheme, a rigorous, mathematical treatment of the recursive hypothesis testing architecture, an online estimation of the probability of correct fix, and the ability to resolve the integer ambiguity with required integrity in minimum time based on the assumed residual statistics.

The possibility of a false fix has prompted researchers to develop analytical fault detection methods [8–10], as well examine other sensors to enhance DGPS such as pseudolites [11]. The pseudolite was not examined as an applicable solution due to a requirement for large geometry change between the tanker and receiver to provide significant levels of integrity. The possibility of supplementing the GPS/INS solution with radio ranging is considered as a direct extension of the EO results presented here because range measurements may be deduced from the EO images.

C. Electro-Optical Sensors

Vision measurements include camera systems, infrared beacon systems, combined with position sensitive diodes, and radar or lidar systems. The measurement outputs of this type of system are a set of bearings measurements (elevation and azimuth) from the EO sensor to the located reference point and possibly a range measurement. Reference-point matching and state-estimation algorithms are suggested in both Valasek et al. [12] and Chiuso et al. [13]. Valasek et al. [12] suggest the use of active beacons on the imaged receiver

target, whereas Chiuso et al. [13] use a passive approach toward identification. Valasek et al. [12] used a least-squares filter to estimate the EO sensor relative position and attitude of the target in view, whereas Chiuso et al. [13] used an EKF structure. Neither related the EO measurements to the inertial sensors. Alternatively, pattern-matching schemes, which attempt to overlay a two-dimensional silhouette of the imaged object onto the image of the target, can be used to produce estimates of relative range, bearings, and attitude. A similar method was used by Boeing as part of the Orbital Express Project to enable satellite on-orbit rendezvous as discussed by Weismuller and Leinz [14].

Both techniques were examined in this research. Reference-point matching requires that the EO sensor contains intelligence to identify key reference points such as special markings, intersection of joints, or even active beacons on the target. Silhouette matching is used to track larger or shapes with more irregular features, including the entire vehicle shape, but requires more computational power to identify, orient, and match the silhouette. Only the reference-point matching results are presented.

A new method for integrating the EO sensors from either technique within the GPS/INS GEKF is developed. The algorithm uses a modified gain extended Kalman filter (MGEKF) [15] to translate the elevation and azimuth angles from reference points or silhouette-matching algorithms to a position error in the camera frame using the known physical relationship between the camera, GPS, IMU, and reference points on the target. Attitude and range measurements are processed using a linearized model about the nominal. Using this method, it is possible to relate the EO measurements to the inertial states of each vehicle within a common inertial reference frame, enabling correction of the relative navigation state with either EO or GPS measurements. The details of the algorithm are presented in the next section.

III. Relative Navigation with Inertial Systems

The primary sensor used for this relative navigation formulation is the strapdown inertial measurement unit providing three-axis acceleration and angular rate measurements. An IMU measures the local acceleration and angular rate at a particular location on the aircraft. The navigation state of each aircraft is calculated at the IMU location. A wireless communication system enables at least one vehicle to share the IMU measurements with the other so that both sets of IMU measurements are available for processing. This section defines the navigation state and the associated error growth of the relative navigation state using two IMUs.

A. Strapdown Equations of Motion

The IMU derives measurements in the inertial reference frame, which, in this paper, is the Earth-centered inertial (ECI) frame. The Earth-centered, Earth-fixed (ECEF) coordinate frame rotates relative to the ECI frame at the Earth's rotation rate ω_{IE}^{E}. The vehicle body frame refers to typical "aircraft coordinates" and consists of orthogonal axes with the x axis positive through the fore of the aircraft, the y axis positive through the starboard side of the aircraft, and the z axis positive down. The local tangent frame is defined using north-east-down coordinates.

The state to be estimated for each vehicle is defined in Eq. (1):

$$x = \begin{bmatrix} P^E \\ V^E \\ Q_B^E \end{bmatrix} \tag{1}$$

The state x consists of the position P^E in the ECEF frame, the velocity V^E in the ECEF frame, and the quaternion Q_B^E defining the body-frame attitude of the vehicle relative to the ECEF frame.

The state is updated in time through integration of the IMU measurements through the strapdown equations of motion defined in Eq. (2):

$$\dot{x} = \begin{bmatrix} \dot{P}^E \\ \dot{V}^E \\ \dot{Q}_B^E \end{bmatrix} = \begin{bmatrix} V^E \\ C_B^E a^B - \omega_{IE}^E \times (\omega_{IE}^E \times P^E) - 2\omega_{IE}^E \times V^E + g^E \\ \frac{1}{2}[\Omega_{EB}^B \times] Q_B^E \end{bmatrix} \tag{2}$$

The matrix C_B^E is the rotation matrix calculated from the quaternion Q_B^E. The quaternion Q_B^E and its interchangeable relationship to the rotation matrix C_B^E may be found in Zipfel [16]. The specific force vector a^B represents the linear specific force measured by the IMU, which includes gravity. The gravity vector g^E is expressed in the ECEF frame. The Earth rotation rate ω_{IE}^E represents the rotation of the ECEF frame relative to the ECI. The quaternion rate matrix $[\Omega_{EB}^B \times]$ is defined as

$$[\Omega_{EB}^B \times] = \begin{bmatrix} 0 & -\omega_x & -\omega_y & -\omega_z \\ \omega_x & 0 & \omega_z & -\omega_y \\ \omega_y & -\omega_z & 0 & \omega_x \\ \omega_z & \omega_y & -\omega_x & 0 \end{bmatrix}; \qquad \omega_{EB}^B = \begin{bmatrix} \omega_x \\ \omega_y \\ \omega_z \end{bmatrix} \tag{3}$$

The angular velocity term ω_{EB}^B represents the angular velocity of the vehicle body frame relative to the ECEF frame represented in the vehicle body frame. The inertial angular velocity ω_{IB}^B is measured by the IMU gyros and consists of the sum of the Earth rotation rate ω_{IE}^E and the rotation of the vehicle body with respect to the ECEF frame, defined as shown in Eq. (4):

$$\omega_{IB}^B = \omega_{IE}^E + \omega_{EB}^B \tag{4}$$

Using these definitions, it is possible to integrate the strapdown equations of motion using the IMU measurements integrated through Eq. (2). A separate state may be established for each vehicle, denoted by x_1 and x_2. The IMU measurements from each vehicle may be integrated to estimate the state of each vehicle, and the difference in the state $\Delta P^E = P_1^E - P_2^E$ is the current estimate of the relative position.

B. Inertial Error Models

The IMU outputs include errors due to imperfections in the sensors. Typical errors include bias, scale factor, and misalignment errors. The study of the error growth in the strapdown equations of motion given in Eq. (2) is given by Britting [17]. In this case, the error models for the accelerometers and rate gyros are reduced to a single error source. This simplified error model is defined in Eq. (5) for accelerometers:

$$\tilde{a}^{\tilde{B}} = C_B^{\tilde{B}} a^B + w_a \tag{5}$$

In this case, the measurement $\tilde{a}^{\tilde{B}}$ is made in the estimated body frame, the true acceleration is defined by a^B and is affected by several error terms. Errors in the estimate of attitude affect the measurement and interpretation of the body-frame acceleration vector measurements. The misalignment between the true body frame and the estimated sensor body frame is represented in a rotation matrix $C_B^{\tilde{B}}$. Errors are represented by w_a and may include scale factor, bias, temperature, or random noise effects.

Likewise, the simplified error models in the angular rate gyro measurements $\tilde{\omega}_{IB}^{\tilde{B}}$ are given in Eq. (6). True angular velocity ω_{IB}^B is modified by the attitude uncertainty $C_B^{\tilde{B}}$ and the errors w_g:

$$\tilde{\omega}_{IB}^{\tilde{B}} = C_B^{\tilde{B}} \omega_{IB}^B + w_g \tag{6}$$

These simplified models may be used to perform a perturbation analysis and determine the effect of the noise and uncertainty on the error growth in the strapdown equations of motion. It is convenient for the present case to ignore scale factor, misalignment, and bias errors.

C. Effects of Errors on the Navigation State

A perturbation approach is take to define the dynamics of the growth of errors in Eq. (2) due to uncertainty caused by w_g and w_a.

The error in the position δP^E and velocity δV^E are defined in Eqs. (7) and (8):

$$\delta P^E = P^E - \bar{P}^E \tag{7}$$

$$\delta V^E = V^E - \bar{V}^E \tag{8}$$

The true position and velocity are defined as P^E and V^E. The current, a priori estimates of position and velocity are $\bar{P}^E$ and $\bar{V}^E$. The error in the true rotation matrix C_B^E is defined as a nonlinear rotation of the a priori estimate of the body to the ECEF $C_{\bar{B}}^E$ frame rotated by the uncertainty in the body frame $C_B^{\bar{B}}$. The relationship is defined in Eq. (9):

$$C_B^E = C_{\bar{B}}^E C_B^{\bar{B}} \tag{9}$$

The term $C_B^{\bar{B}}$ may be defined assuming small angle perturbations in Eq. (10):

$$C_{\bar{B}}^B = \left(I + 2[\delta q_{\bar{B}}^B \times]\right) \tag{10}$$

The quaternion error perturbation $\delta q_{\bar{B}}^B$ is a 3×1 vector representing an assumed small angle rotation.

Using the perturbation error definitions and following the perturbation analysis carried out in Hong et al. [4] or Williamson et al. [1], it is possible to substitute the definitions of Eqs. (7–10) into the strapdown equations of motion defined in Eq. (2) to determine the dynamics of the error growth process. Through elimination of terms of order greater than one, the linearized dynamics of the error are defined in Eq. (11):

$$\begin{bmatrix} \delta\dot{P}^E \\ \delta\dot{V}^E \\ \delta\dot{q}_B^{\bar{B}} \end{bmatrix} = \begin{bmatrix} 0 & I & 0 \\ G - [\omega_{IE}^E \times]^2 & -2[\omega_{IE}^E \times] & -2C_{\bar{B}}^E[\tilde{a}^{\bar{B}} \times] \\ 0 & 0 & -[\tilde{\omega}_{IB}^{\bar{B}} \times] \end{bmatrix} \begin{bmatrix} \delta P^E \\ \delta V^E \\ \delta q_B^{\bar{B}} \end{bmatrix} + \begin{bmatrix} 0 \\ C_{\bar{B}}^E w_a \\ w_g \end{bmatrix} \tag{11}$$

These perturbed dynamics assume knowledge of the gravity gradient G as a function of ECEF position, which is small and negligible for this application. The errors in w_a and w_g are assumed to be zero mean, independent Gaussian noise processes. More complex IMU error models are possible, but are excluded from the current formulation for brevity and clarity. A simple bias may be modeled as a first-order Markov process, as shown in Williamson et al. [1], by augmentation of the Kalman filter state to include terms for w_g and w_a.

The growth in the error of the first vehicle state δx_1 is defined in Eq. (11) and is simplified to the form shown in Eq. (12):

$$\delta\dot{x}_1 = A_1 \delta x_1 + B_1 w_1 \tag{12}$$

In this case, the perturbed error state is defined in Eq. (13):

$$\delta x_1 = \begin{bmatrix} \delta P_1^E \\ \delta V_1^E \\ \delta q_{B1}^{B1} \end{bmatrix} \tag{13}$$

The dynamics matrix A is defined in Eq. (14):

$$A_1 = \begin{bmatrix} 0 & I & 0 \\ G - [\omega_{IE}^E \times]^2 & -2[\omega_{IE}^E \times] & -2C_{\bar{B}1}^E[\tilde{a}_1^{B1} \times] \\ 0 & 0 & -[\tilde{\omega}_{IB1}^{\bar{B}1} \times] \end{bmatrix} \tag{14}$$

The noise sensitivity matrix B is defined in Eq. (15):

$$B_1 = \begin{bmatrix} 0 & 0 \\ C_{\bar{B}1}^E & 0 \\ 0 & I_{3\times 3} \end{bmatrix} \tag{15}$$

The process noise matrix is finally defined in Eq. (16):

$$w_1 = \begin{bmatrix} w_{a1} \\ w_{g1} \end{bmatrix} \tag{16}$$

D. Multivehicle Error Propagation

Because the motion of each vehicle is independent of the other, the error growth should be independent of the other. Integration of each inertial measurement unit will have separate error growth. A combined dynamic system for both vehicles, operating on the state space composed of the state error of vehicle 1 δx_1 with the state error of vehicle 2 δx_2, is presented in Eq. (17). The dynamics and noise sensitivity matrices A_1 and B_1 are calculated using the state estimate of the first vehicle $\bar{x}_1$, whereas the dynamics and noise sensitivity matrix of vehicle 2 (A_2 and B_2) are calculated using the estimate of the second vehicle $\bar{x}_2$:

$$\begin{bmatrix} \delta\dot{x}_1 \\ \delta\dot{x}_2 \end{bmatrix} = \begin{bmatrix} A_1 & 0 \\ 0 & A_2 \end{bmatrix} \begin{bmatrix} \delta x_1 \\ \delta x_2 \end{bmatrix} + \begin{bmatrix} B_1 & 0 \\ 0 & B_2 \end{bmatrix} \begin{bmatrix} w_1 \\ w_2 \end{bmatrix} \tag{17}$$

A simple rotation can be used to redefine the error as shown in Eq. (18) or more simply in Eq. (19), in which the definitions may be inferred from Eq. (18). In this case, $\delta\Delta x = \delta x_1 - \delta x_2$. A similar definition holds for the noise, in which $\Delta w = w_1 - w_2$. The state space of the combined dynamic system is now in terms of the absolute navigation error of vehicle 1 and the relative navigation error between vehicle 1 and vehicle 2. Equation (18) defines the dynamic system used for the GEKF filter structure:

$$\begin{bmatrix} \delta\dot{x}_1 \\ \delta\Delta\dot{x} \end{bmatrix} = \begin{bmatrix} A_1 & 0 \\ A_1 - A_2 & A_2 \end{bmatrix} \begin{bmatrix} \delta x_1 \\ \delta\Delta x \end{bmatrix} + \begin{bmatrix} B_1 & 0 \\ B_1 & -B_2 \end{bmatrix} \begin{bmatrix} w_1 \\ \Delta w \end{bmatrix} \tag{18}$$

$$\delta\dot{x}_{\text{GEKF}} = A_{\text{GEKF}} \delta x_{\text{GEKF}} + B_{\text{GEKF}} w_{\text{GEKF}} \tag{19}$$

The process noise for each inertial system is assumed to be independent of the other. The EKF assumes that each of these noise models is defined by a Gaussian process with statistical properties shown in Eq. (20). The covariance for each IMU noise model is denoted by W_1 and W_2, respectively:

$$\begin{gathered} E\left[\begin{bmatrix} w_1 \\ \Delta w \end{bmatrix}\right] = 0; \qquad E[w_1 w_2^T] = 0 \\ E\left[\begin{bmatrix} w_1 \\ \Delta w \end{bmatrix} [\, w_1 \quad \Delta w \,]\right] = \begin{bmatrix} W_1 & W_1 \\ W_1 & W_1 + W_2 \end{bmatrix} = W_{\text{GEKF}} \end{gathered} \tag{20}$$

Using the statistics for the process noise, the error growth in successive estimates of the strapdown equations of motion can be calculated assuming Gaussian statistics, given initial error covariance P_{GEKF}, consisting of the initial error covariance for each vehicle processed through the rotation previously defined. The initial statistics for the error states are defined in Eq. (21). The discrete time propagation of the global uncertainty, in both the absolute state of vehicle 1 and the relative state, is shown in Eq. (22):

$$\begin{gathered} E\left[\begin{bmatrix} \delta x_1 \\ \delta\Delta x \end{bmatrix}\right] = 0 \\ E\left[\begin{bmatrix} \delta x_1 \\ \delta\Delta x \end{bmatrix} [\, \delta x_1 \quad \delta\Delta x \,]\right] = \begin{bmatrix} P_1 & P_1 \\ P_1 & P_1 + P_2 \end{bmatrix} = P_{\text{GEKF}} \end{gathered} \tag{21}$$

$$M_{\text{GEKF}} = \Phi_{\text{GEKF}} P_{\text{GEKF}} (\Phi_{\text{GEKF}})^T + \Gamma_{\text{GEKF}} W_{\text{GEKF}} \Gamma_{\text{GEKF}}^T \tag{22}$$

The state transition matrix Φ_{GEKF} is defined as $\Phi_{\text{GEKF}} = e^{A_{\text{GEKF}} \Delta t}$, and the discrete time process noise propagation matrix is defined in Eq. (23):

$$\Gamma_{\mathrm{GEKF}} = \int_0^{\Delta t} e^{A_{\mathrm{GEKF}}\tau} B_{\mathrm{EKF}}(\tau)\,\mathrm{d}\tau \tag{23}$$

Successive propagations may be made at each time step Δt by allowing $M_{\mathrm{GEKF}} = P_{\mathrm{GEKF}}$ and repeating at each time step, which forms the GEKF covariance propagation stage.

From Eq. (22), it can be seen that the state error from each IMU grows as a function of time. The drift in the states estimates of the strapdown equations of motion is well understood and described for the single vehicle case in Britting [17]. Other instruments, such as GPS or EO sensors, are required to correct the inertial states of each vehicle and to drive the uncertainty to an acceptable limit. If the amount of time of a particular operation such as aerial refueling is small, then, given a "good" initial condition and very precise inertial sensors, the error in the relative state will grow at a slow rate, which could potentially allow the two vehicles to operate within close proximity until such time as the expected uncertainty exceeds a particular bound. Communication loss can be dealt with by reprocessing the last available IMU measurement, provided the number of packets lost is small, although the covariance should be penalized by the instrument uncertainty and the expected rate of change of acceleration when a data packet is lost. Realistically, the process of generating an appropriate initial condition and real-time relative state estimate requires external calibration from other sensors, such as GPS or EO sensors, especially if each aircraft has been operating for several hours.

IV. Global Positioning System Measurement Correction Model

A GPS receiver measures the position and velocity of the GPS receiver antenna. These measurements may be used to correct an inertial state using a known lever arm between the GPS antenna and the location of the IMU. Transfer of the IMU position estimates P^E_{IMU} to the GPS antenna location P^E_{GPS} for a fixed lever arm requires the vector sum of L_{I2G}, the vector distance from the IMU to the GPS antenna in the vehicle body frame. The relationship for a single vehicle is described in Eq. (24):

$$P^E_{\mathrm{GPS}} = P^E_{\mathrm{IMU}} + C^E_B L_{I2G} \tag{24}$$

To determine the effect of inertial state error on the position at the GPS antenna, Eq. (24) is perturbed and linearized around the current estimate of the inertial state. The resulting GPS measurement function is defined in Eq. (25):

$$\tilde{P}^E_{\mathrm{GPS}} = \bar{P}^E_{\mathrm{GPS}} + C_P \delta x + v \tag{25}$$

The variable $\tilde{P}^E_{\mathrm{GPS}}$ represents the GPS antenna position measurement in the ECEF frame; the term $\bar{P}^E_{\mathrm{GPS}}$ is the a priori estimate of the GPS antenna position based on the inertial navigation state and computed from Eq. (24). The state error δx is the perturbed state error with dynamics defined in Eq. (12). Measurement noise v corrupts the measurement, and the measurement sensitivity matrix C_P is defined in Eq. (26):

$$C_P = \begin{bmatrix} I & 0 & -2C^E_{\tilde{B}}[L_{I2G}\times] \end{bmatrix} \tag{26}$$

The resulting cross-product matrix in Eq. (26) operates on the attitude error in the inertial state error vector and limits the observability of the attitude state estimates.

Note that the present case may be extended to include more precise GPS measurement models. The notation presented here follows Hong et al. [4], which shows how to extend this "loosely" coupled measurement model to a "tightly" coupled measurement model using GPS range measurements. A full measurement model for pseudorange and Doppler is presented in Williamson et al. [1]. The full pseudorange formulation requires that the receiver clock bias for both vehicles be added to the state. A typical model for clock bias and clock drift would require the augmentation of the GEKF state space by four states, two for vehicle 1 and two for the relative clock terms.

A. Differential Measurements

Differential GPS measurements are defined as the difference between two sets of GPS measurements, each from a different GPS receiver. The first receiver is referred to as the base receiver and the second is often referred to as the rover. Differential GPS measurements eliminate error sources common to both receivers, such as ionosphere and troposphere errors. The measurements have high accuracy [18,19] when compared with standard GPS measurements, provided that the two receivers process exactly the same satellite set. High-accuracy code measurements on the order of a meter [2] of error or less can be generated from two GPS receivers. Centimeter level accuracy may be achieved through solving the real-time kinematic (RTK) carrier-phase integer ambiguity problem [2] as described later. Given two sets of GPS position measurements, one for the first vehicle and the other for the second vehicle, the measurement model takes on the form in Eq. (27):

$$\begin{bmatrix} \tilde{P}^E_{\mathrm{GPS1}} \\ \tilde{P}^E_{\mathrm{GPS2}} \end{bmatrix} = \begin{bmatrix} \bar{P}^E_{\mathrm{GPS1}} \\ \bar{P}^E_{\mathrm{GPS2}} \end{bmatrix} + \begin{bmatrix} C_{P1} & 0 \\ 0 & C_{P2} \end{bmatrix} \begin{bmatrix} \delta x_1 \\ \delta x_2 \end{bmatrix} + \begin{bmatrix} b_c \\ b_c \end{bmatrix} + \begin{bmatrix} v_1 \\ v_2 \end{bmatrix} \tag{27}$$

The measurement function for each vehicle is dependent upon the a priori state estimates of the position and attitude. Two separate lever arms L_{I2G1} and L_{I2G2} are defined for each vehicle because the distance from the IMU to GPS antenna will likely be different on both vehicles. The algorithm assumes that both lever arms are precisely known. The a priori state estimate $\bar{P}^E_{\mathrm{GPS1}}$ is calculated using the state of the first vehicle $\bar{x}_1$ and associated lever arm L_{I2G1}, whereas $\bar{P}^E_{\mathrm{GPS2}}$ is calculated using the state of the first vehicle $\bar{x}_2$ and associated lever arm L_{I2G2}, each according to Eq. (24). The matrices C_{P1} and C_{P2} are each calculated using Eq. (26) using the respective state and lever arm. The measurement noise terms v_1 and v_2 represent receiver-specific error sources and are independent of each other. The measurements in Eq. (27) are corrupted by the same common mode errors b_c. Using the same rotation employed to change the dynamics in Eq. (18), the relative state errors may be modified to the following form:

$$\begin{bmatrix} \tilde{P}^E_{\mathrm{GPS1}} \\ \Delta\tilde{P}^E_{\mathrm{GPS}} \end{bmatrix} = \begin{bmatrix} \bar{P}^E_{\mathrm{GPS1}} \\ \Delta\bar{P}^E_{\mathrm{GPS}} \end{bmatrix} + \begin{bmatrix} C_{P1} & 0 \\ C_{P1} - C_{P2} & C_{P2} \end{bmatrix} \begin{bmatrix} \delta x_1 \\ \delta\Delta x \end{bmatrix} + \begin{bmatrix} b_c \\ 0 \end{bmatrix} + \begin{bmatrix} v_1 \\ \Delta v \end{bmatrix} \tag{28}$$

The differential measurement $\Delta\tilde{P}^E_{\mathrm{GPS}} = \tilde{P}^E_{\mathrm{GPS1}} - \tilde{P}^E_{\mathrm{GPS2}}$ defines the measurement created by differencing the output of two receivers. The rotation removes the effect of the common mode errors in the differential measurements.

B. Differential Carrier-Phase and Integer Ambiguity

The differential carrier-phase measurements provide information about the relative distance between each GPS antenna to centimeter level once the RTK problem of resolving the integers is solved. Refer to Hofmann-Wellenhof et al. [19] for a discussion of the derivation of double-difference carrier-phase measurements and error sources. A double-difference carrier-phase measurement is calculated for the purpose of eliminating the common mode errors and the clock bias. The double difference is defined as in Eq. (29):

$$\nabla\Delta\tilde{\phi} = \tilde{\phi}^i_1 - \tilde{\phi}^j_1 - (\tilde{\phi}^i_2 - \tilde{\phi}^j_2) \tag{29}$$

In this case, satellite i and satellite j each represent different satellites currently in view by both receivers 1 and 2. The combination of four different measurements of the form in Eq. (30) results in a single measurement corrupted only by position estimate error and the receiver tracking error noise:

$$\lambda(\nabla\Delta\tilde{\phi} + \nabla\Delta N) = \nabla\Delta\bar{\rho} + \left(C^i_{\mathrm{LOS}} - C^j_{\mathrm{LOS}}\right)\Delta\delta P^E_{\mathrm{GPS}} + \nabla\Delta v_\phi \tag{30}$$

In this case, the double-differenced integer number of wavelengths between the receiver and satellite is $\nabla\Delta N$, the a priori double-differenced estimate of the range to the satellite is $\nabla\Delta\bar{\rho}$, the carrier wavelength is λ, and the double-difference receiver noise is $\nabla\Delta v_\phi$. The line-of-sight (LOS) matrix C^i_{LOS} from receiver 1 to satellite i is defined in Eq. (31). It is assumed in Eq. (30) that the line-of-sight matrix from either receiver to a particular satellite is equivalent, which is approximately true for receivers within 10–20 km of each other:

$$C^i_{\text{LOS}} = \frac{\left(P^E_i - \bar{P}^E_{1\text{GPS}}\right)^T}{\left\|P^E_i - \bar{P}^E_{1\text{GPS}}\right\|} \tag{31}$$

The method presented in this paper assumes that another algorithm provides a solution to the integer ambiguity $\nabla\Delta N$. Many algorithms exist for performing this function. The method used for this application was the multiple hypotheses Wald sequential probability ratio test presented in Wolfe et al. [2].

Once the integer ambiguity is estimated, an EKF is constructed to process the double-differenced carrier-phase measurements along with the relative GPS measurements. The GEKF measurement model uses the form shown in Eq. (32):

$$\begin{bmatrix} \tilde{P}^E_{\text{GPS1}} \\ \Delta\tilde{P}^E_{\text{GPS}} \\ \lambda(\nabla\Delta\tilde{\phi} + \nabla\Delta N) \end{bmatrix} = \begin{bmatrix} \bar{P}^E_{\text{GPS1}} \\ \Delta\bar{P}^E_{\text{GPS}} \\ \nabla\Delta\bar{\rho} \end{bmatrix} + \begin{bmatrix} C_{P1} & 0 \\ C_{P1} - C_{P2} & C_{P2} \\ \nabla C_{\text{LOS}}(C_{P1} - C_{P2}) & \nabla C_{\text{LOS}} C_{P2} \end{bmatrix} \begin{bmatrix} \delta x_1 \\ \delta\Delta x \end{bmatrix} + \begin{bmatrix} b_c \\ 0 \\ 0 \end{bmatrix} + \begin{bmatrix} v_1 \\ \Delta v \\ \nabla\Delta v_\phi \end{bmatrix} \tag{32}$$

The measurement noise for Eq. (32) is assumed to be Gaussian with statistics defined in Eq. (33):

$$E\left[\begin{bmatrix} b_c + v_1 \\ \Delta v \\ \nabla\Delta v_\phi \end{bmatrix}\right] = 0$$

$$E\left[\begin{bmatrix} b_c + v_1 \\ \Delta v \\ \nabla\Delta v_\phi \end{bmatrix}\begin{bmatrix} b_c + v_1 & \Delta v & \nabla\Delta v_\phi \end{bmatrix}\right] = \begin{bmatrix} V_{bc} + V_1 & V_1 & 0 \\ V_1 & V_1 + V_2 & 0 \\ 0 & 0 & V_\phi \end{bmatrix} = V_{\text{GEKF}} \tag{33}$$

The measurement sensitivity matrix is lumped together into a common matrix defined as shown in Eq. (34):

$$C_{\text{GEKF}} = \begin{bmatrix} C_{P1} & 0 \\ C_{P1} - C_{P2} & C_{P2} \\ \nabla C_{\text{LOS}}(C_{P1} - C_{P2}) & \nabla C_{\text{LOS}} C_{P2} \end{bmatrix} \tag{34}$$

Note that this model is generic with respect to different carrier-phase wavelengths: L1, L2, wide lane, narrow lane, or any other linear combination. These measurements may be modified to include double-differenced code measurements as previously stated or to use single-differenced code or Doppler measurements, provided that the state is augmented to incorporate receiver clock error models for both receivers.

C. Correction of the Inertial State

This measurement function can now be used as part of the GEKF to estimate the navigation state errors for both vehicles. Whenever a GPS measurement is available, the inertial states $\bar{x}_1$ and $\bar{x}_2$ are propagated forward to the time of validity of the GPS measurements using the method outlined in Eq. (2). The covariance M_{GEKF} is propagated using the covariance calculated from Eq. (22). Then, the GPS measurements are used to correct the state using the EKF structure. The covariance is updated using the EKF covariance update formula in Eq. (35), and the Kalman gain is calculated in Eq. (36):

$$P_{\text{GEKF}} = M_{\text{GEKF}} - M_{\text{GEKF}} C^T_{\text{GEKF}} (C_{\text{GEKF}} M_{\text{GEKF}} C^T_{\text{GEKF}} + V_{\text{GEKF}})^{-1} C_{\text{GEKF}} M_{\text{GEKF}} \tag{35}$$

$$K = P_{\text{GEKF}} C^T_{\text{GEKF}} V^{-1}_{\text{GEKF}} \tag{36}$$

A state correction can be calculated using Eq. (37):

$$\begin{bmatrix} \delta\hat{x}_1 \\ \delta\Delta\hat{x} \end{bmatrix} = K\left(\begin{bmatrix} \tilde{P}^E_{\text{GPS1}} \\ \Delta\tilde{P}^E_{\text{GPS}} \\ \lambda(\nabla\Delta\tilde{\phi} + \nabla\Delta N) \end{bmatrix} - \begin{bmatrix} \bar{P}^E_{\text{GPS1}} \\ \Delta\bar{P}^E_{\text{GPS}} \\ \nabla\Delta\bar{\rho} \end{bmatrix}\right) \tag{37}$$

The correction is applied to the state estimate after each GPS measurement using the following method. The complete error state is repeated in Eq. (38):

$$\begin{bmatrix} \delta\hat{x}_1 \\ \delta\Delta\hat{x} \end{bmatrix} = \begin{bmatrix} \delta P^E_1 \\ \delta V^E_1 \\ \delta q^{B1}_{B1} \\ \delta P^E_1 - \delta P^E_2 \\ \delta V^E_1 - \delta V^E_2 \\ \delta q^{B1}_{B1} - \delta q^{B2}_{B2} \end{bmatrix} \tag{38}$$

The error estimates for each vehicle represented in Eq. (38) are separated using a simple linear transformation. First, vehicle 1 is corrected and then vehicle 2 is corrected. The inertial navigation state is updated separately using the process defined in Eqs. (39–42). First, the position and velocity are updated directly using the following perturbations:

$$\hat{P}^E = \bar{P}^E + \delta\hat{P}^E \qquad \hat{V}^E = \bar{V}^E + \delta\hat{V}^E \tag{39}$$

The attitude is corrected using a nonlinear process. First, a complete quaternion is created from the perturbed quaternion correction using the quaternion constraint equation to define the missing term:

$$\hat{Q}^{\bar{B}}_{\hat{B}} = \begin{bmatrix} \bar{q}_0 \\ \delta\hat{q} \end{bmatrix} \tag{40}$$

The variable $\bar{q}_0$ is given in Eq. (41):

$$\bar{q}_0 = \sqrt{1.0 - \delta q_1^2 - \delta q_2^2 - \delta q_3^2} \tag{41}$$

The a priori estimate of attitude is corrected using the updated quaternion through a quaternion rotation:

$$Q^E_{\hat{B}} = Q^E_{\bar{B}} \otimes Q^{\bar{B}}_{\hat{B}} \tag{42}$$

Alternatively, the same process may be performed by first converting each quaternion into a cosine rotation matrix and performing a standard multiplication to form a new rotation matrix, and then converting this back to a quaternion or Euler angles. Refer to Zipfel [16] for details of the calculation of a quaternion rotation. In either case, care should be taken to properly normalize the quaternion during correction as well as integration through Eq. (2).

The process continues as the inertial state $\bar{x}$ for each vehicle is propagated using the strapdown equations of motion in Eq. (2). Because the state correction $\delta\hat{x}$ is applied to the inertial state $\bar{x}$ after each GPS measurement, there is no need to propagate the error state through the linearized dynamics.

Note that, if both vehicles are flying in formation in a straight and level manner, the dynamics and measurement models may be

reduced. Essentially, $A_1 \approx A_2$ in Eq. (18) and $C_{P1} \approx C_{P2}$ in Eq. (32), causing the base vehicle state and the relative state to approximately decouple. This notion was used to generate a reduced-order filter used in the Autonomous Formation Flight experiment [1]. However, given sufficient processing power, the GEKF method presented here is superior, especially when $A_1 \neq A_2$, which occurs even during simple dynamics such as when the vehicles are in a turn.

V. Electro-Optical Measurements

An EO sensor operates on one vehicle and is used to image and provide measurements of the location of another vehicle in the EO sensor frame. This EO system may be, for instance, used on the tanker to image an aircraft receiving fuel. Typical EO measurements come in one of two forms. Either the EO system provides bearings measurements (elevation and azimuth) from the sensor to a reference point on the imaged vehicle, or the sensor attempts to perform pattern matching between the image of the vehicle and a set of recorded images. The first method is referred to as reference-point mapping. The second method is referred to as silhouette matching because the EO sensor attempts to match a possibly three-dimensional model to a two-dimensional image by first projecting the 3-D model onto the assumed image plane and forming the 2-D silhouette.

A lever arm is defined that relates the location of the EO sensor relative to the INS in the tanker vehicle body frame. Additional lever arms are defined on the receiver aircraft that locate each of the reference points relative to the receiver INS in the receiver body frame. It is assumed that these lever arms are known a priori.

The measurement model of the vision system is defined relative to the inertial system on each system. The relative position between the camera and a given reference point is defined in terms of the relative position between each IMU in the ECEF coordinate frame as

$$\Delta P^E_{iC} = P^E_i - P^E_C = P^E_{\text{IMU2}} + C^E_{\tilde{B}_2} L^{\tilde{B}_2}_{2-i} - P^E_{\text{IMU1}} - C^E_{\tilde{B}_1} L^{\tilde{B}_1}_{1-C} \quad (43)$$

In this case, the position of the EO sensor or camera in the ECEF coordinate frame is P^E_C, the position of the reference point i on the target in the ECEF coordinate frame is P^E_i, and the relative position vector ΔP^E_{iC} is the difference between the two vectors $\Delta P^E_{iC} = P^E_i - P^E_C$. The relative position vector may be defined in terms of the receiver vehicle IMU state P^E_{IMU2} in the ECEF coordinate frame plus the lever arm between the IMU and the reference location $L^{\tilde{B}_2}_{2-i}$, which must be rotated from the vehicle body frame into the ECEF frame using the cosine rotation matrix $C^E_{\tilde{B}_2}$. Likewise, the tanker vehicle's IMU position is defined as P^E_{IMU1} and is located relative to the camera system through the lever arm $L^{\tilde{B}_1}_{1-C}$ rotated from the primary vehicle body frame to the ECEF coordinate frame through cosine rotation matrix $C^E_{\tilde{B}_1}$. The sensor model developed relates the camera system to the inertial reference frame defined by the IMU. Using this relationship, a measurement error model is constructed which incorporates the GEKF state estimates and enables the integration of the camera system within the existing GPS/INS GEKF structure.

The relative position from camera to image reference point vector in the camera frame is defined as

$$\Delta P^C_{iC} = \begin{bmatrix} \Delta X^C_{iC} \\ \Delta Y^C_{iC} \\ \Delta Z^C_{iC} \end{bmatrix} = \begin{bmatrix} x^C_1 - x^C_{2i} \\ y^C_1 - y^C_{2i} \\ z^C_1 - z^C_{2i} \end{bmatrix} \quad (44)$$

Each of the terms is one component of the relative position vector between the camera lens and the reference point on the receiver related in the camera reference frame. The camera frame is defined such that the x axis points out of the camera lens, the y axis points to starboard, and the z axis points down.

A. Bearings-Only Measurement Model

Passive EO systems may provide angle or bearings measurements from the tanker to a reference point on the receiver. Each reference point may take the form of an active beacon on the viewed vehicle or a small, recognizable portion of the vehicle with known location relative to the inertial system. This form of blending is referred to as "tightly coupled" GPS/INS/EO-based processing because minimal processing is typically required for reference point identification. Bearings measurements are made of two angles defined as

$$\begin{bmatrix} \tilde{\alpha}_{iC} \\ \tilde{\beta}_{iC} \end{bmatrix} = \begin{bmatrix} \tan^{-1}\left(\frac{\Delta Z^C_{iC}}{\Delta X^C_{iC}}\right) \\ \tan^{-1}\left(\frac{\Delta Y^C_{iC}}{\Delta X^C_{iC}}\right) \end{bmatrix} + \begin{bmatrix} \upsilon_\alpha \\ \upsilon_\beta \end{bmatrix} \quad (45)$$

In this case, α_{iC} represents the elevation angle of the reference point i relative to the camera C in the camera frame, and β^C_{iC} represents the azimuth angle of the target. The additive noise terms are assumed zero mean, Gaussian with noise variance associated with the error models including pixel noise and blurring effects. Each measurement pair represents the relative azimuth and elevation of one reference point on the target vehicle relative in the camera frame.

Bearings measurements are in the spherical coordinate frame, whereas the relative navigation state is in Cartesian coordinates. The MGEKF [15] translates the elevation and azimuth angles to a Cartesian position error in the camera frame. The modified form, which is shown in [15] improves steady-state error through a sophisticated linearization process. The error in the bearings measurements in the camera frame is defined as follows. The derivation is presented in Appendix A.

$$\begin{bmatrix} \tilde{\alpha}_{iC} - \bar{\alpha}_{iC} \\ \tilde{\beta}_{iC} - \bar{\beta}_{iC} \end{bmatrix} = H_{\text{MGEKF}i} H_{\text{LOS}_i} \begin{bmatrix} x^C_1 - x^C_{2i} \\ y^C_1 - y^C_{2i} \\ z^C_1 - z^C_{2i} \end{bmatrix} \quad (46)$$

The matrix $H_{\text{MGEKF}i}$ is defined in Eq. (A5), and the line-of-sight matrix of the vision reference point H_{LOS_i} is defined in Eq. (A6). The relative position vector measurement model in terms of the GEKF state is defined in Eq. (47) by taking perturbations in Eq. (43) and using these perturbations to relate the error in the navigation state to the errors in the camera frame, as discussed in Appendix A. The matrix H_{1-C} shown in Eq. (47) is defined in Eq. (A18):

$$\begin{bmatrix} \tilde{\alpha}_{iC} \\ \tilde{\beta}_{iC} \end{bmatrix} - \begin{bmatrix} \bar{\alpha}_{iC} \\ \bar{\beta}_{iC} \end{bmatrix} = H_{\text{MGEKF}i} H_{\text{LOS}-i} H_{1-C} \begin{bmatrix} \delta x_1 \\ \delta \Delta x \end{bmatrix} + \begin{bmatrix} \upsilon_\alpha \\ \upsilon_\beta \end{bmatrix} \quad (47)$$

The measurement model in Eq. (47) is sufficient to provide relative navigation solutions to the GEKF previously defined. Instead of using differential GPS or differential carrier-phase GPS measurements, the solution may use bearings measurements to estimate corrections to the relative navigation state. Complete observability of the relative navigation state requires that sufficient reference points are available (at least three) with sufficient geometry to estimate the relative navigation state. Sufficient geometry of reference points is achieved if H_{1-C} has appropriate rank, which may be designed offline. Sufficient observability in real time requires that the combined matrix $H_{\text{MGEKF}} H_{\text{LOS}}$ for all visible reference points has sufficient rank, which takes into account the present separation distance of the two vehicles. Note that partial observability of the absolute attitude errors in vehicle 1 is achieved because the measurements are placed within a common inertial frame.

B. Including Range and Attitude in the Measurement Model

On occasion, a separate processor may image the target and provide an estimate of the range, bearings, and even relative attitude between the target and the camera in the camera frame. This type of output is typical in "silhouette matching" techniques such as the algorithm discussed by Weismuller and Leinz [14]. A method is presented to relate these measurements to the state space of the GEKF. This process may be defined as "loosely coupled" because it uses the output of a separate process as inputs to the GEKF, similar to using loosely coupled differential GPS measurements. The terminology of loosely coupled and tightly coupled for EO sensor fusion is patterned after GPS/INS definitions. The relative position and attitude measurement vector is defined as $\tilde{y}_i$, where i still denotes

a particular location on the imaged target to which the relative position corresponds:

$$\tilde{y}_{\mathrm{LC}i} = \begin{bmatrix} \tilde{\rho}_i \\ \tilde{\alpha}_i \\ \tilde{\beta}_i \\ \tilde{Q}^C_{B_2} \end{bmatrix} \tag{48}$$

In this case, $\tilde{\alpha}_i$ and $\tilde{\beta}_i$ have the same angle definition as before. The new variable $\tilde{\rho}_i$ represents the scalar range from the vision system to the target along the vector line defined by $\tilde{\alpha}_i$ and $\tilde{\beta}_i$. The quaternion $\tilde{Q}^C_{B_2}$ is the estimated attitude of the target relative to the camera system.

The simplified EO measurement model is derived in Appendix B. The result is shown in Eq. (49), in which the sensitivity matrix H_{EO} is defined in Eq. (B11) and the noise covariance V_{EO} is defined in Eq. (B10):

$$\tilde{r}_{\mathrm{LC}i} = \begin{bmatrix} \tilde{\rho}_i - \bar{\rho}_i \\ \tilde{\alpha}_i - \bar{\alpha}_i \\ \tilde{\beta}_i - \bar{\beta}_i \\ r_q \end{bmatrix} = H_{\mathrm{EO}} \begin{bmatrix} \delta x_1 \\ \delta \Delta x \end{bmatrix} + V_{\mathrm{EO}} \tag{49}$$

Note that the preceding model assumes that vehicle 1 images vehicle 2 using either reference points or silhouette matching. However, it is trivial to expand the results to include additional measurement of vehicle 2 imaging vehicle 1. Further, multiple silhouettes may be generated for different parts of the vehicle in view. Using either bearings only with multiple reference points or a silhouette-matching scheme, or combinations thereof, it is possible to use the measurement models defined in Eq. (49) and/or Eq. (47) to correct the inertial errors with error modeling defined in Eq. (18).

C. Correcting the Inertial with Electro-Optics

The GEKF presented previously for GPS/INS sensor fusion is now modified to include the vision system measurements. The inertial navigation state is propagated forward in time by an amount Δt using the strapdown equations of motion in Eq. (2), and the covariance is propagated using Eq. (22). At that time, if GPS measurements are available, the navigation state may be updated and corrected using the GPS measurement function and EKF corrections outlined in Eqs. (35–42). If the EO sensor measurements are available, then the EKF can be calculated using the appropriate covariance propagation and update equations for the EO sensor models presented to generate the Kalman gain K for the EO measurements. The state correction is then calculated using the residual and the appropriate gain as shown in Eq. (52):

$$P_{\mathrm{GEKF}} = M_{\mathrm{GEKF}} - M_{\mathrm{GEKF}} H^T_{\mathrm{EO}} \times (H_{\mathrm{EO}} M_{\mathrm{GEKF}} H^T_{\mathrm{EO}} + V_{\mathrm{EO}})^{-1} H_{\mathrm{EO}} M_{\mathrm{GEKF}} \tag{50}$$

$$K_{\mathrm{EO}} = P_{\mathrm{GEKF}} H^T_{\mathrm{EO}} V^{-1}_{\mathrm{EO}} \tag{51}$$

$$\begin{bmatrix} \delta \hat{x}_1 \\ \delta \Delta \hat{x} \end{bmatrix} = K_{\mathrm{EO}} \left(\begin{bmatrix} \tilde{\rho}_i - \bar{\rho}_i \\ \tilde{\alpha}_i - \bar{\alpha}_i \\ \tilde{\beta}_i - \bar{\beta}_i \\ r_q \end{bmatrix} \right) \tag{52}$$

No a priori estimate of the error needs to be maintained because the correction is applied to the state estimate immediately. The same correction process is applied as in Eqs. (39–42). Note that this correction may take place at a rate different than the GPS measurements. The INS data are used to propagate the state and error covariance to the time of validity of either the GPS or EO measurements. Corrections are made at the GPS or EO measurement time of validity. The scheme provided is generic and will operate with an instrument that provides a measurement of range, relative attitude, or bearings, such as radio ranging, radar, or radio beacon navigation.

VI. Experimental Results

A series of tests were conducted in a hardware-in-the-loop simulation to validate the GEKF in various modes of operation. For each test, the relative position output of the GEKF was differenced with a truth vector calculated within the HITL simulation. Results show that the relative position error was maintained to within 10 cm per axis using a combination of either GPS/INS or GPS/INS/EO sensors. The goal of the experiment was to demonstrate the sensor fusion process in real time and to automatically maneuver a robotic boom model into an aircraft model receptacle based on the output of the navigation solution.

A. Hardware-in-the-Loop Test Facility

The hardware-in-the-loop facility is a robotic facility designed to simulate boom-receptacle refueling operations. The facility is depicted in Fig. 2. The right picture shows the facility as a whole. The left picture is a close up of the robotic aircraft and boom. The aircraft and boom are one-eighth scale models. A motion control system moves the aircraft in three axes of translation. Another motion control system extends and pivots the boom to change the boom elevation and azimuth angles. The aircraft is equipped with a receptacle capable of interconnecting with the boom.

In this experiment, the algorithms presented for relative navigation were implemented on a real-time computer system with wireless communication. This real-time navigation hardware consisted of two formation flight instrumentation system (FFIS) units, each with its own GPS receiver (Ashtech Z-12) and inertial measurement unit interface, using synchronous data link control (a common serial IMU interface). One FFIS unit is assumed to be attached to each vehicle. The receiver aircraft FFIS processes data from the receiver aircraft GPS receiver and IMU. These data are then transmitted to the tanker over a wireless (802.11g) data link. The tanker FFIS unit receives vision-based data from a camera system imaging the receiver aircraft, along with the output of the tanker GPS (Z-12) and IMU. After calculating the relative state, the boom control system maneuvers the boom to couple with the receiver aircraft using the navigation output from the tanker FFIS. The block diagram of the HITL is depicted in Fig. 3.

Encoders on the motion control system provided true position measurements of the receiver aircraft and the boom. A computer, called the navigation simulation computer (NSC), calculated truth relative position of the aircraft and tanker states using outputs from the motion control encoders.

The NCS computer produced outputs emulating the IMU measurements for each vehicle on a serial bus. The NCS also transmitted the true state of each vehicle to a GPS constellation simulator. The constellation simulator generates the actual RF signals a real GPS receiver would experience at the transmitted navigation state. The constellation simulator also generated 1 pulse-per-second that provided timing for the NCS and actuation control system. Each FFIS processed the IMU measurements from the NCS, and each FFIS GPS receiver processed the RF signals from the constellation simulator. Timing on the FFIS was regulated by the local GPS receiver output.

The EO systems were integrated into the HITL to provide real-time EO updates. A near-infrared (IR) spectrum camera was placed underneath the boom, nearly equivalent to a boom operator's view of the refueling scenario. The IR camera was a Sensors Unlimited InGaAs SWIR MiniCamera with windowing. The camera was sampled using a National Instruments data acquisition card. A set of fixed IR lamps were placed on the receiver aircraft. Each lamp burned at the same frequency. The lights were not modulated. Software was developed to process the incoming image and identify each lamp through comparisons with the known geometry. These measurements were converted to bearings measurements and delivered to the FFIS for processing. Six beacons were used and depicted in Fig. 4.

Fig. 2 Scale model of an F-16 as a receiver aircraft with boom (left). Complete HITL facility (right).

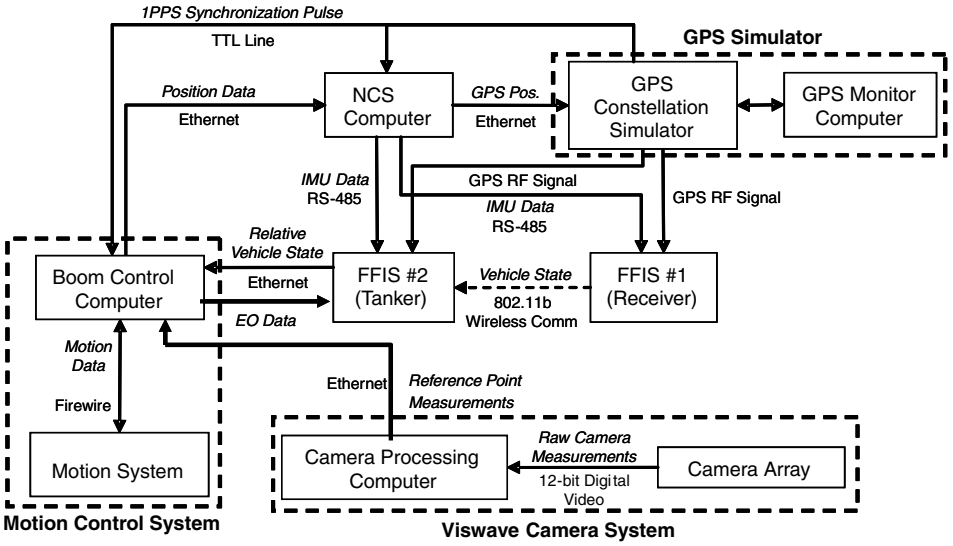

Fig. 3 HITL block diagram.

The plus signs and numbering system were added onto the image to highlight the beacons for this report.

B. Simulation Models

The NCS computer used the actuators of the robotic aircraft and boom to define the relative position, velocity, acceleration, and attitude, and to simulate the tanker state. The tanker was simulated in software in real time, flying at an altitude of 6100 m on a due west heading with a velocity of 123 m/s. The receiver aircraft trajectory was calculated by adding the tanker flight condition onto a relative state estimate derived from the robotic aircraft model. The location of the model was measured using the actuator encoders sampled at 100 Hz. The precision of the actuator encoders translated to less than 0.2 mm of translational travel. A simple Kalman filter (KF) estimated the relative position, velocity, and acceleration of the aircraft model relative to the boom-receptacle point using the encoder measurements. The receiver state was formed as the sum of the simulated tanker state and the relative state estimate scaled up to the true aircraft size. The inertial measurement unit was assumed to be at the center of the navigation point. IMU measurements were generated from the estimated trajectories. The receiver aircraft model did not rotate relative to the tanker. Figure 5 shows the relative trajectory in the tanker body frame in meters for 100 s. This trajectory was representative of the motion simulated for multiple experiments.

An EO camera was used to estimate the position and attitude of the aircraft in the camera frame. Because the location of the camera was known and fixed, it was possible to compare the EO position estimates with the actuator position estimates, which were shown to be within agreement to within 0.5 mm. A least-squares algorithm was constructed to estimate the relative position and attitude from the six beacons on the aircraft model, and was used to calibrate the location of each beacon. The system was calibrated against the actuation system and verified with an independent IR beacon solution provided by Phase Space. Note that the Phase Space system requires

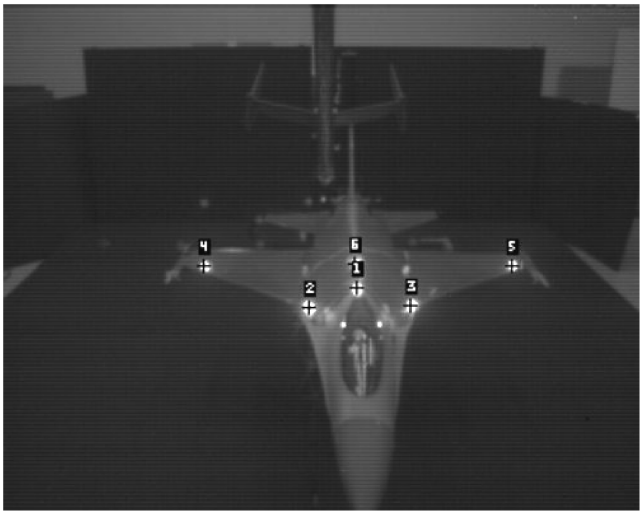

Fig. 4 Receiver aircraft with instrumented IR lamps. Highlights and numbers added to the image to clarify lamp locations.

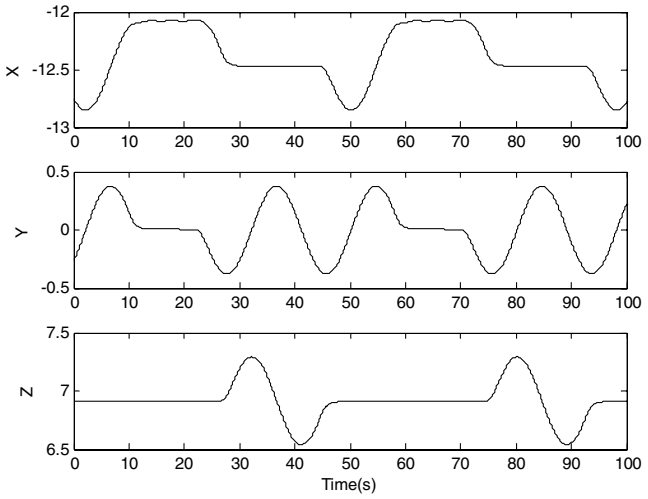

Fig. 5 Full-scale relative position trajectory between tanker and receiver in tanker body frame in meters.

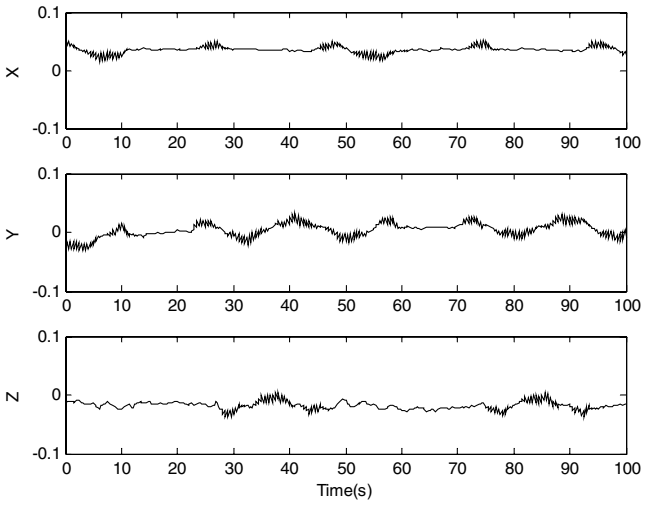

Fig. 6 Least-squares DCP GPS solution error relative to actuation system in meters.

specialized timing beacons that operate in sequence, whereas the beacons used for the real-time experiment did not have any special signal structure.

The state of each vehicle simulated or estimated was transmitted to the GPS constellation simulator at 100 Hz over Ethernet. The state corresponded to the GPS antenna location. The GPS simulator generated RF signals for L1 and L2 frequencies, which were processed by the Ashtech Z-12 GPS receivers. The GPS receiver output measurements at 2 Hz. The Wald test described previously was used to resolve the integer ambiguity between the tanker and receiver aircraft. Figure 6 shows the error in the least-squares GPS solution and the KF tracking the actuator encoders in the tanker body frame in meters. Remarkably, the combined errors from the actuator estimation through the constellation simulator remain less than a few centimeters when converted to full aircraft scale. The plot does show a slight bias in the longitudinal direction, which was caused by slight timing variations in the system.

The location and lever arms of each sensor on the receiver aircraft are listed in Table 1 in the receiver body frame, including the GPS antenna location and the location of each of the six infrared beacons. Table 2 shows the location of instruments on the tanker in the tanker body frame, including GPS antenna, EO sensor location, and EO sensor orientation with respect to the tanker body frame. The orientation angles are in degrees. For each aircraft, the IMU defined the origin for the body frame.

The GEKF operated on the tanker FFIS. The process noise parameters are listed in Table 3. The process noise model included a GPS clock bias and a random walk bias for each accelerometer and rate gyro in the same way as described in Williamson et al. [1]. The GEKF processed IMU data at 10 Hz through the strapdown equations of motion. GPS code range, Doppler, and differential carrier-phase measurements were processed at 2 Hz. The EO measurements of azimuth and elevation of each beacon were also processed at 2 Hz. The EO measurements were time aligned with the GPS measurements. The simple KF attempted to estimate the IMU measurements at a time synchronized with GPS, but due to the nature of the robotic actuation system, timing synchronization with GPS could only be guaranteed to within 5 ms. The GEKF measurement noise standard deviations are listed in Table 4. The EO error accuracy was derived based on the pixel size and range to target. Each beacon was visible through a minimum of six pixels throughout the test. With the selected camera, the standard deviation of the centroid of the beacon would be approximately 2 cm per axis at 50 ft separation from the camera at full scale.

Table 1 Receiver aircraft sensor lever arm locations in meters at full scale

Sensor	Location	
IR beacon #1	X	2.639
	Y	0.139
	Z	−0.237
IR beacon #2	X	2.063
	Y	1.212
	Z	4.659
IR beacon #3	X	2.004
	Y	−1.213
	Z	0.424
IR beacon #4	X	−0.687
	Y	4.069
	Z	0.411
IR beacon #5	X	−0.769
	Y	−4.489
	Z	0.415
IR Beacon #6	X	0.816
	Y	0.032
	Z	−0.167
GPS antenna	X	3.000
	Y	0.000
	Z	−1.000

Table 2 Tanker aircraft sensor lever arm locations in meters at full scale

Sensor	Location	
EO sensor	X	4.476
	Y	0.59
	Z	1.266
EO orientation	Yaw	181.42
	Pitch	−22.2
	Roll	−0.5
GPS antenna	X	3
	Y	0
	Z	−1

Table 3 GEKF process noise parameters

Process noise	Value	Units
Acceleration	0.01	m/s
Angular rate	1	deg /h
Acceleration random walk	0.001	$\mathrm{m}/\sqrt{\mathrm{s}^3}$
Gyro random walk	0.001	$\mathrm{deg}/\sqrt{\mathrm{s}}$
Clock bias	0.01	m
Clock drift	0.1	m/s
Clock acceleration	0.01	m/s/s

Table 4 GEKF measurement noise parameters

Measurement	Value	Units
Beacon elevation	0.001	rad
Beacon azimuth	0.001	rad
GPS psuedorange	5	m
GPS Doppler	0.1	m/s
GPS carrier phase	0.02	m

C. Validation Test Results

The results of using three different filters are examined. The three filter types are differential carrier-phase GPS with inertial, EO with inertial, and combined GPS and EO. The relative position error is shown for all three cases in Fig. 7. The relative attitude error is shown in Fig. 8. The dashed line represents the differential carrier GPS case. The dashed-dot line represents the EO-only case, and the solid line represents the combined filter. For the EO-only filter case, the tanker GPS code and Doppler GPS measurements are still processed to stabilize the base vehicle state. The GPS-only results show similar bias and tracking performance as the least-squares GPS results depicted in Fig. 6, which is to be expected. The combined results show similar performance, indicating that the filter is currently weighing the GPS more heavily than the EO.

D. Feedback Control

The outputs of the relative estimate were fed back to the boom control, and the boom was able to automatically "plug" the moving

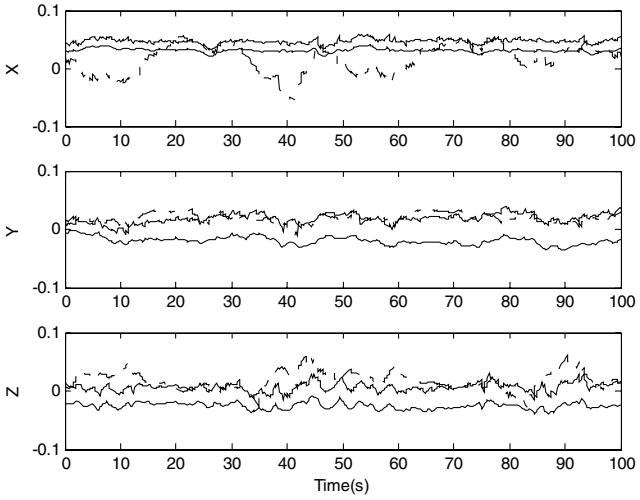

Fig. 7 Relative position error in tanker body frame for the three filter cases.

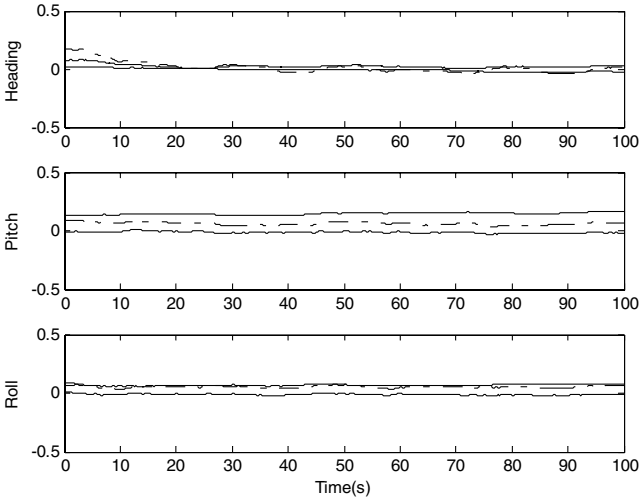

Fig. 8 Relative attitude errors for the three filter cases.

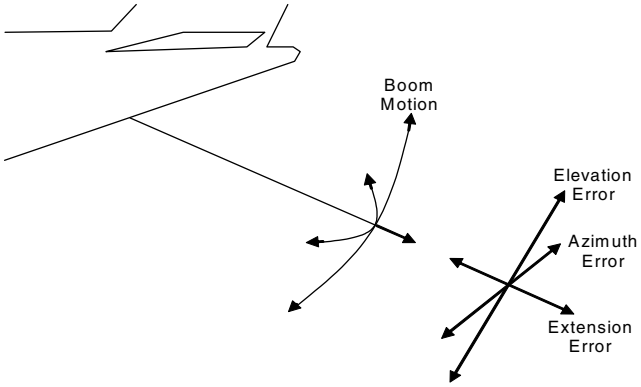

Fig. 9 Boom control system coordinate frame.

receiver using only navigation data provided from the FFIS. A control law was developed to operate on the navigation solution to guide the boom into the receptacle. The control law used the tanker navigation state estimates to translate the tanker IMU location to the boom tip location. The boom position was measured relative to the tanker using the boom motion control encoders. The control law also translated the receiver IMU to the known receiver receptacle location to generate the relative position of the boom tip and the receiver receptacle. This relative position was translated into spherical coordinates of elevation, azimuth, and boom extension. Figure 9 shows the boom coordinate frame.

The boom control laws produced a tracking error on the elevation and azimuth axes of less than 0.05 m, adequate for automated refueling. To estimate tracking error, an "ideal" boom position is calculated using the true F-16 receptacle position and converting it to the boom coordinate frame. Figure 10 shows the tracking error between the actual and ideal boom position showing that the navigation system provided adequate control authority to plug the receptacle.

VII. Conclusions

A method for fusing measurements from Global Positioning System receivers, inertial measurement units, and electro-optical sensors is presented and applied to estimating the relative position, velocity, and attitude between two vehicles. The inertial states are propagated in time using the inertial measurements processed through the strapdown equations of motion. The Global Positioning System measures position in the ECEF frame to provide corrections to the inertial state of each vehicle and enable very precise corrections of the relative state between the vehicles. The electro-optical sensors measure position in the spherical coordinate frame and can provide equally precise corrections to the relative navigation state. The methodology presented shows seamless integration of both sensor types to correct inertial errors, despite disparities in instrument type and installation locations. A real-time test, simulating an automated aerial refueling scenario, demonstrated that the electro-optical and Global Positioning System measurements could be fused through an extended Kalman filter process so that the navigation function would operate to correct the inertial states with both sets of measurements or either set of measurements if one set fails. The system is therefore redundant in relative navigation function. Test results show the real-time capability to estimate relative positions to centimeter level using the defined methodology. Initial studies indicate that the accuracy is available to automate boom refueling functions and that redundancy in basic navigation function is achieved, improving system safety.

Appendix A: Derivation of Tightly Coupled Electro-Optical Measurement Model

The error function for the tightly coupled bearings and azimuth measurements (in the EO sensor frame) is now defined. First, the residual process is defined as the difference between the measured and a priori estimates of the angles:

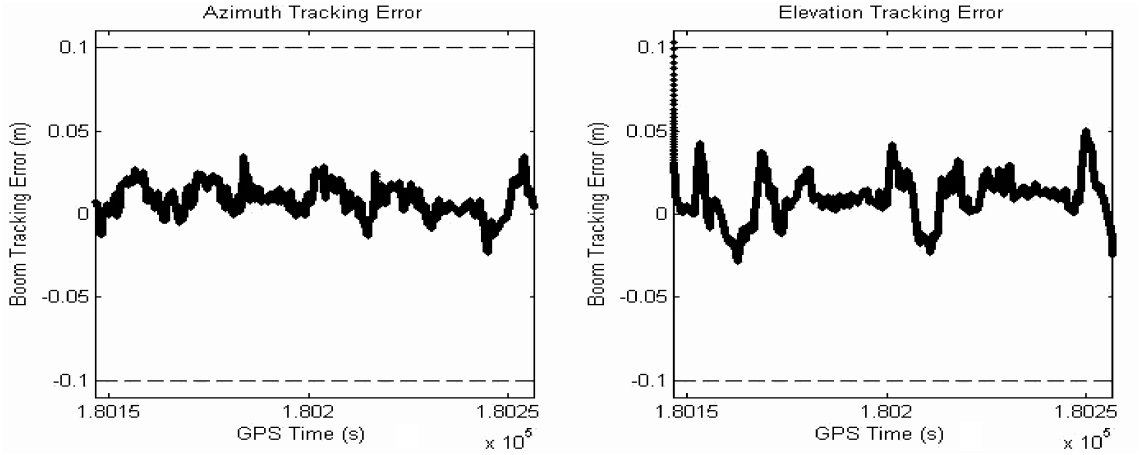

Fig. 10 Boom control system tracking error.

$$r_i = \begin{bmatrix} \alpha_i - \bar{\alpha}_i \\ \beta_i - \bar{\beta}_i \end{bmatrix} = \begin{bmatrix} \tan^{-1}\left(\frac{z_1^C - z_{2i}^C}{x_1^C - x_{2i}^C}\right) - \tan^{-1}\left(\frac{\bar{z}_1^C - \bar{z}_{2i}^C}{\bar{x}_1^C - \bar{x}_{2i}^C}\right) \\ \tan^{-1}\left(\frac{y_1^C - y_{2i}^C}{x_1^C - x_{2i}^C}\right) - \tan^{-1}\left(\frac{\bar{y}_1^C - \bar{y}_{2i}^C}{\bar{x}_1^C - \bar{x}_{2i}^C}\right) \end{bmatrix} \triangleq \begin{bmatrix} \tan^{-1}(\Theta) \\ \tan^{-1}(\Psi) \end{bmatrix} \tag{A1}$$

In Eq. (A1), we define the angles Θ and Ψ using the following relationship:

$$\tan^{-1}(a) - \tan^{-1}(b) = \tan^{-1}\left(\frac{a-b}{1+ab}\right) \tag{A2}$$

Therefore, the residual process may be rewritten in the following way [15]:

$$r_i = \begin{bmatrix} \tilde{\alpha}_i - \bar{\alpha}_i \\ \tilde{\beta}_i - \bar{\beta}_i \end{bmatrix} = \begin{bmatrix} -D_1 \tan^{-1}(\Theta)/\Theta & 0 \\ 0 & -D_2 \tan^{-1}(\Psi)/\Psi \end{bmatrix} \times \begin{bmatrix} \sin(\tilde{\alpha}_i) & 0 & -\cos(\tilde{\alpha}_i) \\ \sin(\tilde{\beta}_i) & -\cos(\tilde{\beta}_i) & 0 \end{bmatrix} \begin{bmatrix} x_1^C - x_{2i}^C \\ y_1^C - y_{2i}^C \\ z_1^C - z_{2i}^C \end{bmatrix} \tag{A3}$$

where

$$\begin{aligned} D_1 &= 1/[\cos(\tilde{\alpha}_i)(\bar{x}_1^C - \bar{x}_{2i}^C) + \sin(\tilde{\alpha}_i)(\bar{z}_1^C - \bar{z}_{2i}^C)] \\ D_2 &= 1/[\cos(\tilde{\beta}_i)(\bar{x}_1^C - \bar{x}_{2i}^C) + \sin(\tilde{\beta}_i)(\bar{y}_1^C - \bar{y}_{2i}^C)] \end{aligned} \tag{A4}$$

We define the modified gain for the measurement function as

$$H_{\text{MGEKF}i} = \begin{bmatrix} -D_1 \tan^{-1}(\Theta)/\Theta & 0 \\ 0 & -D_2 \tan^{-1}(\Psi)/\Psi \end{bmatrix} \tag{A5}$$

The line-of-sight matrix formed directly from the measurements is

$$H_{\text{LOS}_i} = \begin{bmatrix} \sin(\tilde{\alpha}_i) & 0 & -\cos(\tilde{\alpha}_i) \\ \sin(\tilde{\beta}_i) & -\cos(\tilde{\beta}_i) & 0 \end{bmatrix} \tag{A6}$$

The error in the bearings measurements in the camera frame may now be written as

$$\begin{bmatrix} \tilde{\alpha}_i - \bar{\alpha}_i \\ \tilde{\beta}_i - \bar{\beta}_i \end{bmatrix} = H_{\text{MGEKF}i} H_{\text{LOS}_i} \begin{bmatrix} x_1^C - x_{2i}^C \\ y_1^C - y_{2i}^C \\ z_1^C - z_{2i}^C \end{bmatrix} \tag{A7}$$

To relate the measurements to the inertial error for each vehicle, the relative position vector is first calculated relative to the inertial frames through the camera frame, defined in Eq. (44). Perturbations are taken around the relative state vector in Eq. (A8):

$$\begin{aligned} \Delta P_{iC}^C &= C_{B_1}^C C_E^{B_1}\left(P_i^E - P_C^E\right) \\ &= C_{B_1}^C C_E^{B_1}\left(P_2^E + C_{B_2}^E L_{2-i}^{B_2} - P_1^E - C_{B_1}^E L_{1-C}^{B_1}\right) \end{aligned} \tag{A8}$$

In this case, the lever arms $L_{2-i}^{B_2}$ and $L_{1-C}^{B_1}$ are assumed known, as is the orientation of the camera relative to the inertial system on vehicle 1 C_{B1}^E.

Perturbations in the position and attitude of each vehicle are defined in Eqs. (A9–A12):

$$P_1^E = \bar{P}_1^E + \delta P_1 \tag{A9}$$

$$P_2^E = \bar{P}_2^E + \delta P_2 \tag{A10}$$

$$C_{B1}^E = C_{\bar{B}1}^E\left(I + 2\left[\delta q_{B1}^{\bar{B}1}\times\right]\right) \tag{A11}$$

$$C_{B2}^E = C_{\bar{B}2}^E\left(I + 2\left[\delta q_{B2}^{\bar{B}2}\times\right]\right) \tag{A12}$$

These perturbations are substituted back into Eq. (A8) to form the relative state with error sourced in Eq. (A13):

$$\begin{aligned} \Delta P_{iC}^C = {} & C_{B1}^C(I - 2[\delta q_1\times])C_E^{\bar{B}_1}\left(\bar{P}_2^E + \delta P_2 - \bar{P}_1^E - \delta P_1\right) - C_{B_1}^C L_{1-C}^{B_1} \\ & + C_{B_1}^C(I - 2[\delta q_1\times])C_E^{\bar{B}_1} C_{\bar{B}_2}^E(I + 2[\delta q_2\times])L_{2-i}^{B2} \\ & - \left[C_{B_1}^C C_E^{\bar{B}1}\left(\bar{P}_2^E - \bar{P}_1^E\right) - C_{B1}^C L_{1-C}^{B1} + C_{B1}^C C_E^{\bar{B}_1} C_{\bar{B}2}^E L_{2-i}^{B2}\right] \end{aligned} \tag{A13}$$

Regrouping the terms of Eq. (A13) into the GEKF state space and excluding higher-order terms of perturbations produces Eq. (A14):

$$\Delta P_{iC}^C \approx \Delta \bar{P}_{iC}^C + C_{B1}^C[0 \quad 0 \quad H_{Q1} \quad C_E^{\bar{B}1} \quad 0 \quad (H_{Q1} + H_{Q2})] \begin{bmatrix} \delta P_1 \\ \delta V_1 \\ \delta q_{B1}^{\bar{B}1} \\ \Delta\delta P \\ \Delta\delta V \\ \Delta\delta q \end{bmatrix} \tag{A14}$$

The a priori estimate $\Delta \bar{P}_{iC}^C$ is defined in Eq. (A15):

$$\Delta \bar{P}_{iC}^C = C_{B_1}^C C_E^{\bar{B}_1}\left(\bar{P}_2^E + C_{\bar{B}_2}^E L_{2-i}^{B_2} - \bar{P}_1^E - C_{\bar{B}_1}^E L_{1-C}^{B_1}\right) \tag{A15}$$

The term H_{Q1} is defined in Eq. (A16):

$$H_{Q1} = 2\left(\left[C_E^{\bar{B}_1}(\bar{P}_1^E - \bar{P}_2^E)\times\right] + \left[\left(C_E^{\bar{B}_1} C_{\bar{B}_2}^E L_{2-i}^{B2}\right)\times\right]\right) \tag{A16}$$

The term H_{Q2} is defined in Eq. (A17):

$$H_{Q2} = 2C_E^{\bar{B}1} C_{\bar{B}_2}^E \left[\left(L_{2-i}^{B_2}\right)\times\right] \tag{A17}$$

The most notable portion of Eq. (A14) is the fact that, because the camera measurements are related through the inertial frame, the term H_{Q1} actually provides limited observability of the error in the absolute state of vehicle 1. In other words, the absolute state of vehicle 1 relative to the Earth is observable through the camera measurements. This additional observability is a direct result of the fact that the camera measurements, which provide only relative state information, are related through a common inertial reference frame.

Therefore, we define the matrix H_{1-C} in Eq. (A18):

$$H_{1-C} = C_{B1}^C \begin{bmatrix} 0 & 0 & H_{Q1} & C_E^{\bar{B}1} & 0 & (H_{Q1} + H_{Q2}) \end{bmatrix} \tag{A18}$$

Appendix B: Derivation of Loosely Coupled Electro-Optical Measurement Model

This section outlines a method for relating relative position in spherical coordinates and a relative attitude estimate to the relative position in Cartesian coordinates and relative attitude in the inertial space. Position measurements in spherical coordinates include range, elevation angle, and azimuth angle relative to the camera. This section applies to correcting inertial data using a loosely coupled EO sensor, operating a silhouette-matching technique to estimate the relative position and attitude between the two vehicles. Equation (B1) defines the measurement processed.

$$\tilde{y}_i = \begin{bmatrix} \tilde{\rho}_i \\ \tilde{\alpha}_i \\ \tilde{\beta}_i \\ \tilde{Q}_{B_2}^C \end{bmatrix} \tag{B1}$$

The bearings measurements $\tilde{\alpha}_i$ and $\tilde{\beta}_i$ are defined as azimuth and elevation, respectively. The variable $\tilde{\rho}_i$ represents the scalar range from the camera system to the target along the vector line defined by $\tilde{\alpha}_i$ and $\tilde{\beta}_i$. The quaternion $\tilde{Q}_{B_2}^C$ is the estimated attitude of the target relative to the camera system.

The a priori relative range measurement is calculated as the norm of the relative state vector, or

$$\bar{\rho} = \|\Delta P_{iC}^C\| \tag{B2}$$

Here, the range measurement matrix $H_{\rho i}$ is defined as

$$H_{\rho i} = \begin{bmatrix} \frac{\Delta \bar{X}_{iC}^C}{\|\Delta P_i^C\|} & \frac{\Delta \bar{Y}_{iC}^C}{\|\Delta P_i^C\|} & \frac{\Delta \bar{Z}_{iC}^C}{\|\Delta P_i^C\|} \end{bmatrix} \tag{B3}$$

The combined bearings measurement matrices are equivalent to the previous forms as

$$\begin{bmatrix} H_{C\alpha} \\ H_{C\beta} \end{bmatrix} = H_{\text{MGEKF}} H_{\text{LOS}_i} \tag{B4}$$

The matrix H_{1-C} is defined as in Eq. (A18).

The error from the attitude is treated separately because the residual is a set of relative attitude angles and is not related to the relative distance as the range, azimuth, and elevation are related to range. The attitude determined from an image defines the rotation from the vehicle body frame of the imaged vehicle to the camera frame. The measurement function is nonlinear, as shown in Eq. (B5):

$$\tilde{C}_{B_2}^C = C_{\bar{B}_2}^C (I + 2[\delta q_2\times])(I + [v_q\times]) \tag{B5}$$

In this case, the term $\tilde{C}_{B_2}^C$ is the rotation matrix determined from the estimated relative yaw, pitch, and roll of the imaged vehicle in the camera produced image. The a priori estimate of the rotation is $C_{\bar{B}_2}^C$.

Two errors are associated with the rotation. The first is due to the error in the estimate of the imaged vehicle. This is composed of the usual attitude quaternion perturbation δq_2. An additional, nonlinear rotation error is due to errors in the image processing v_q. The measurement equation may be rewritten in terms of a linearized residual in which higher-order terms of the rotation error and noise are neglected:

$$r_q = \begin{bmatrix} \left(\tilde{C}_{\bar{B}_2}^C C_C^{\bar{B}_2}\right)_{32} \\ \left(\tilde{C}_{\bar{B}_2}^C C_C^{\bar{B}_2}\right)_{13} \\ \left(\tilde{C}_{\bar{B}_2}^C C_C^{\bar{B}_2}\right)_{21} \end{bmatrix} = H_q \begin{bmatrix} \delta x_1 \\ \delta \Delta x \end{bmatrix} + \begin{bmatrix} v_\Phi \\ v_\Theta \\ v_\Psi \end{bmatrix} \tag{B6}$$

In this case, the form $(\tilde{C}_{\bar{B}_2}^C C_C^{\bar{B}_2})_{ij}$ is the ith row and jth column of the 3×3 matrix $\tilde{C}_{\bar{B}_2}^C C_C^{\bar{B}_2}$.

The quaternion measurement matrix H_q is simply defined in Eq. (B7):

$$H_q = [0 \quad 0 \quad 2I \quad 0 \quad 0 \quad -2I] \tag{B7}$$

The measurement noise v_q is decomposed into the axial components as

$$v_q = \begin{bmatrix} v_\Phi \\ v_\Theta \\ v_\Psi \end{bmatrix} \tag{B8}$$

Therefore, the residual is formed using Eq. (B6) and the associated error models. The error models are then used to form and correct the GEKF already defined. The total measurement error model for relative position in spherical coordinates is

$$\begin{bmatrix} \tilde{\rho}_i - \bar{\rho}_i \\ \tilde{\alpha}_i - \bar{\alpha}_i \\ \tilde{\beta}_i - \bar{\beta}_i \\ r_q \end{bmatrix} = \begin{bmatrix} H_{\rho i} H_{1-C} \\ H_{C\alpha} H_{1-C} \\ H_{C\beta} H_{1-C} \\ H_q \end{bmatrix} \begin{bmatrix} \delta x_1 \\ \delta \Delta x \end{bmatrix} + \begin{bmatrix} v_\rho \\ v_\alpha \\ v_\beta \\ v_q \end{bmatrix} \tag{B9}$$

The measurement noise is assumed to be Gaussian with the following statistics:

$$E\left[\begin{bmatrix} v_\rho \\ v_\alpha \\ v_\beta \\ v_q \end{bmatrix}\right] = 0; \qquad E\left[\begin{bmatrix} v_\rho \\ v_\alpha \\ v_\beta \\ v_q \end{bmatrix} [v_\rho \quad v_\alpha \quad v_\beta \quad v_q]\right] = V_{\text{EO}} \tag{B10}$$

Note that V_{EO} is a covariance which contains any and all of the correlations between the noise processes, as determined by the method used to generate the range, angles, and attitude measurements. It is up to the designer to select appropriate values for V_{EO}. Likewise, the measurement sensitivity is grouped together into a single matrix for convenience of notation:

$$H_{\text{EO}} = \begin{bmatrix} H_{\rho i} H_{1-C} \\ H_{C\alpha} H_{1-C} \\ H_{C\beta} H_{1-C} \\ H_q \end{bmatrix} \tag{B11}$$

Therefore, the simplified measurement for loosely coupled measurements is defined in the following equation:

$$\tilde{r}_{\text{LC}i} = \begin{bmatrix} \tilde{\rho}_i - \bar{\rho}_i \\ \tilde{\alpha}_i - \bar{\alpha}_i \\ \tilde{\beta}_i - \bar{\beta}_i \\ r_q \end{bmatrix} = H_{\text{EO}} \begin{bmatrix} \delta x_1 \\ \delta \Delta x \end{bmatrix} + V_{\text{EO}} \tag{B12}$$

Acknowledgment

The authors wish to acknowledge Boeing Advanced Aerial Refueling Systems in Long Beach, California for their support of this work.

References

[1] Williamson, W. R., Abdel-Hafez, M. F., Rhee, I., Wolfe, J. D., Chichka, D. F., and Speyer, J. L., "An Instrumentation System Applied to Formation Flight," *IEEE Transactions on Control Systems Technology*, Vol. 15, No. 1, Jan. 2007, pp. 75–85. doi:10.1109/TCST.2006.883241

[2] Wolfe, J. D., Williamson, W. R., and Speyer, J. L., "Hypothesis Testing for Resolving Integer Ambiguity in GPS," *Journal of Navigation*, Vol. 50, No. 1, 2003, pp. 45–56.

[3] Williamson, W. R., Abdel-Hafez, M. F., Rhee, I., Wolfe, J. D., and Speyer, J. L., "A Formation Flight Experiment Using Differential Carrier Phase for Precise Relative Navigation," *Proceedings of the 15th International Technical Meeting of the Satellite Division of the Institute of Navigation ION GPS 2002*, Inst. of Navigation, Fairfax, VA, 2002, pp. 988–1001.

[4] Hong, S., Lee, M. H., Rios, J., and Speyer, J. L., "Observability Analysis of GPS Aided INS," *Proceedings of the 13th International Technical Meeting of the Satellite Division of the Institute of Navigation*, Inst. of Navigation, Fairfax, VA, 2000, pp. 2618–2624.

[5] Williamson, W. R., Real Time, High Accuracy, Relative State Estimation for Multiple Vehicle Systems, Ph.D. Thesis, Univ. of California, Los Angeles, 2000.

[6] Teunissen, P. J. G., De Jonge, P. J., and Tiberius, C. C. J. M., "Performance of the LAMDA Method for Fast GPS Ambiguity Resolution," *Navigation: Journal of the Institute of Navigation*, Vol. 44, No. 3, 1997, pp. 373–383.

[7] Pervan, B., Chan, F. C., Gebre-Egziabher, D., Pullen, S., Enge, P., and Colby, G., "Performance Analysis of Carrier-Phase DGPS Navigation for Shipboard Landing of Aircraft," *Navigation: Journal of the Institute of Navigation*, Vol. 50, No. 3, 2003, pp. 181–191.

[8] Chan, S., and Speyer, J. L., "A Sequential Probability Test for RAIM," *Proceedings of the 17th International Technical Meeting of the satellite division of the Institute of Navigation*, Inst. of Navigation, Fairfax, VA, 2004, pp. 1798–1802.

[9] Malladi, D., and Speyer, J. L., "A Generalized Shiryayev Sequential Probability Ratio Test for Change Detection and Isolation," *IEEE Transactions on Automatic Control*, Vol. 44, No. 8, Aug. 1999, pp. 1522–1534. doi:10.1109/9.780416

[10] Mutuel, L. H., and Speyer, J. L., "Fault-Tolerant Estimator Design for a UAV," *Proceedings of the 2000 AIAA Guidance, Navigation, and Control Conference*, AIAA 2000-4464, 2000.

[11] Pervan, B. S., Cohen, C., and Parkinson, B. W., "Integrity Monitoring for Precision Approach Using Kinematic GPS and a Ground-Based Pseudolite," *Journal of Navigation*, Vol. 41, No. 2, 1994, pp. 159-174.

[12] Valasek, J., Kimmett, J., Hughes, D., Gunnam, K., and Junkins, J. L., "Vision Based Sensor and Navigation System for Autonomous Aerial Refueling," *AIAA 1st UAV Conference*, AIAA 2002-3441, 2002.

[13] Chiuso, A., Favaro, P., Jin, H., and Soatto, S., "Structure from Motion Causally Integrated over Time," *IEEE Transactions on Pattern Analysis and Machine Intelligence*, Vol. 24, No. 4, April 2002, pp. 523–535. doi:10.1109/34.993559

[14] Weismuller, T., and Leinz, M., "GN&C Technology Demonstrated by the Orbital Express Autonomous Rendezvous and Capture Sensor System," Presented at the *29th Annual American Astronautical Society Guidance and Control Conference*, American Astronautical Society 06-016, Feb. 2006.

[15] Wolfe, J. D., and Speyer, J. L., "Target Association Using Detection Methods," *Journal of Guidance, Control, and Dynamics*, Vol. 25, No. 6, Nov.–Dec. 2002, pp. 1143–1148. doi:10.2514/2.4994

[16] Zipfel, P., *Modeling and Simulation of Aerospace Vehicle Dynamics*, AIAA, Reston, VA, 2000, pp. 121–128.

[17] Britting, K., *Inertial Navigation Systems Analysis*, Wiley-Interscience, New York, 1971.

[18] Parkinson, B. W., and Spiker, J. J., *Global Positioning System: Theory and Applications*, Vols. 1–2, AIAA, Reston, VA, 1996.

[19] Hofmann-Wellenhof, B., Lichtenegger, H., and Collins, J., *GPS Theory and Practice*, 4th ed., Springer–Verlag, New York, 1997.